

Contents lists available at [ScienceDirect](https://www.sciencedirect.com)

Journal of Petroleum Science and Engineering

journal homepage: www.elsevier.com/locate/petrol

Shear-thinning or shear-thickening fluid for better EOR? — A direct pore-scale study

Chiyu Xie^a, Weifeng Lv^{b,c}, Moran Wang^{a,*}^a Department of Engineering Mechanics and CNMM, Tsinghua University, Beijing 100084, China^b Department of Polymer Science and Engineering, School of Chemistry and Chemical Engineering, Nanjing University, Nanjing 210023, China^c Research Institute of Petroleum Exploration & Development, CNPC, Beijing 100083, China

ARTICLE INFO

Keywords:

Multiphase flow
 Non-Newtonian fluid
 Diversion effect
 Lattice Boltzmann method
 Porous media
 Enhanced Oil Recovery (EOR)

ABSTRACT

Non-Newtonian fluids are widely applied in Enhanced Oil Recovery (EOR) techniques, and the good performances have been ascribed to the shear-thinning or shear-thickening characteristics of them. In this paper, we aim at discovering the roles of these rheological properties in non-Newtonian fluid displacement from the pore scale. A recently developed lattice Boltzmann model (LBM) for multiphase viscoplastic fluid flow [Xie et al. *J Non-Newton Fluid*, 2016.234: 118–128] is used. Displacements in both homogeneous and heterogeneous porous media are considered. For homogeneous cases, the performances of shear-thinning and shear-thickening fluids are almost the same when compared in favorable displacement regime; while the performance of shear-thinning fluid is poorer than that of shear-thickening fluid in unfavorable displacement regime. For heterogeneous cases, we demonstrate that the shear-thinning property does not contribute too much to the diversion effect, which clarifies the debate of understandings. Our pore-scale modeling results also indicate the significance of low viscosity ratio for diversion and EOR, which can stabilize the displacing front despite of the increased viscous resistance.

1. Introduction

Currently, there is still a large portion of remaining oil being trapped in most reservoirs due to unfavorable conditions like heterogeneity and ultra-low permeability. To overcome these difficulties and obtain as much oil as possible, several Enhanced Oil Recovery (EOR) techniques have been applied (Alvarado and Manrique, 2010; Thomas, 2008). Among these techniques, polymer flooding (Abdulbaki et al., 2014; AlSofi and Blunt, 2010; He et al., 2008; Jung et al., 2013; Liu et al., 2015b; Wang et al., 2000; Wei et al., 2014) and foam displacement (Al Ayesh et al., 2016; Andrianov et al., 2012; Farajzadeh et al., 2010; Talebian et al., 2014; Zhang et al., 2000) are two of the most popular methods. Both of them are reported to have the capabilities of increasing sweep efficiency, controlling the mobility or viscosity ratio, and diverting the displacing fluid from higher-permeability layer to lower-permeability (diversion effect) (Al Ayesh et al., 2016; Bai et al., 2015; Li et al., 2010; Yan et al., 2006).

For EOR mechanisms, the elasticity property of some polymers can help pull and strip the remaining oil (Wang et al., 2000; Wei et al., 2014; Zhang et al., 2011), and the polymer solutions usually have high viscosities to suppress the fingering-type displacement. For foams, their low

surface tension property can reduce the flow resistance (Farajzadeh et al., 2010), and their viscosities are also high. Moreover, most of the polymers and foams are easy to deform under shear force during displacement. As a result, their rheology properties usually behave like viscoplastic non-Newtonian fluids as well, whose viscosities change with shear rate. For example, foams are considered as shear-thinning fluids, since the rearrangement ability to relax the shear stress applied on them. While for various kinds of polymers, both shear-thinning and shear-thickening behaviors are observed (Wever et al., 2011).

Therefore, it is quite necessary to understand the roles of shear-thinning and shear-thickening properties in EOR. However, there seems to still have some debates on which category is better. As early as 1980, Jones (1980) pointed out that shear-thickening is better for stratified rocks with various permeabilities, while shear-thinning is better under uniform displacement front conditions. Zhu et al. (1998) thought that the shear-thinning property of foam allow for lower injection pressures near the highly sheared wellbore area. Zhang et al. (2000) supposed that the shear rate in a large pore throat is lower than in a small pore throat, thus shear-thinning could lead to a relative smaller resistance in low permeable core and contribute greater oil recovery in heterogeneous reservoir. Al Ayesh et al (Al Ayesh et al., 2016). indicated the

* Corresponding author.

E-mail address: mrwang@tsinghua.edu.cn (M. Wang).

important role of shear-thinning behavior in foam diversion. On the contrary, Delshad et al. (2008). supposed that the shear-thickening property of polymer could help to displace the still mobile but hard-to-displace oil faster or to effectively displace the bypassed oil in small-scale heterogeneities. AlSofi and Blunt (2010) constructed a streamline-based simulation to prove that shear-thinning could reduce sweep efficiency and recovery. Their conclusions were reasonable through the comparisons between the recovery by a Newtonian fluid flooding and by a shear-thinning fluid with lower apparent viscosity; however the performance of the shear-thinning fluid with a higher apparent viscosity was not reported.

Although it is not comprehensive enough so far, direct pore-scale methods like OpenFOAM (Raeni et al., 2014) and lattice Boltzmann method (LBM) (Huang et al., 2015; Liu et al., 2015a; Xie et al., 2016a; Xie et al., 2016b; Zhu and Ma, 2013) have offered an alternative powerful way for revealing flow physics in porous media. Nevertheless, few relevant studies on this specific issue have been found, besides some indirect investigations on single-phase non-Newtonian fluid flow in porous media (Morais et al., 2009; Ohta et al., 2011).

In this work, we aim to strictly investigate and compare the performances of shear-thinning and shear-thickening fluids as displacing fluids for EOR at the pore scale, excluding other interference factors like viscoelasticity, the setting of a reference viscosity, etc. A multiphase LBM model for viscoplastic fluid (Xie et al., 2016b) recently developed from a phase-field LBM model for Newtonian fluid (Shao et al., 2014) is applied. This model is able to capture the momentum evolution and yielded regions well in two-phase non-Newtonian flow. The localized treatment of shear rate in this LBM model can improve the efficiency and accuracy over other direct simulators, thus make it suitable as well for direct flow simulations in porous media.

The rest parts of this paper are organized as follows. In Section 2, we will describe the governing equations and will review the multiphase viscoplastic LBM scheme briefly. Additionally, the domain set-up and boundary conditions will be illustrated. In Section 3, shear-thinning fluid and shear-thickening fluid flooding through both homogeneous and heterogeneous samples will be investigated, comparing with water flooding results. Their diversion capabilities will be compared in the heterogeneous displacement part. Finally, we will draw our conclusion in Section 4.

2. Numerical methods

2.1. Governing equations

In order to capture the fluid flow at pore scale, we directly solve the Navier-Stokes equation instead of using the Darcy's law. To describe the interfacial dynamics for two-phase interaction, the Cahn-Hilliard equation (Cahn and Hilliard, 1958) is applied for its better physical understanding from the essence of free-energy theory. Moreover, the constitutive relation (Herschel and Bulkley, 1926) to deal with the shear behavior of viscoplastic fluid is required. Therefore, the governing equations in this work are:

$$\nabla \cdot (\rho \mathbf{u}) = 0, \quad (1)$$

$$\partial_t (\rho \mathbf{u}) + (\mathbf{u} \cdot \nabla) \rho \mathbf{u} = -\nabla \cdot p \mathbf{I} + \rho \nu \nabla^2 \mathbf{u} - \phi \nabla \cdot \lambda \mathbf{I} + \mathbf{F}, \quad (2)$$

$$\partial_t \phi + \mathbf{u} \cdot \nabla \phi = M_\phi \nabla^2 \lambda, \quad (3)$$

$$\tau \geq \tau_y : \quad \tau = \tau_y + K \dot{\gamma}^n. \quad (4)$$

Here, \mathbf{u} is velocity vector, t is time, ρ is the local fluid density, p is the hydrodynamic pressure, \mathbf{I} is the identity tensor, ν is the local kinematic viscosity, \mathbf{F} is the body force term; $\phi = (\rho_1 - \rho_2)/2$ is the order parameter to distinguish two phases with density ρ_1 and ρ_2 , λ is the chemical potential, M_ϕ is the interface mobility which controls the diffusion rate of

interface (Huang et al., 2009); τ is the shear stress, $\dot{\gamma}$ is the shear rate; τ_y is the yield shear stress, K is the consistency index, and n is the flow index. The Cahn-Hilliard equation (3) for interface description and the Navier-Stokes equation (2) for fluid hydrodynamics are linked by the term “ $-\phi \nabla \cdot \lambda \mathbf{I}$ ” in Eq. (2). This term is an extra force originating from the interfacial dynamics, which is closely related to interface tension σ and contact angle θ .

2.2. The multiphase viscoplastic LBM model

A recently developed multiphase LBM model for viscoplastic fluid (Xie et al., 2016b) is adopted to solve the above equations in porous media. Two sets of LB equations are derived for the recovery of continuous equation (1), Navier-Stokes equation (2) and Cahn-Hilliard equation (3) as

$$f_i(\mathbf{x} + \mathbf{c}_i \Delta t, t + \Delta t) - f_i(\mathbf{x}, t) = -\frac{1}{\tau_f} (f_i(\mathbf{x}, t) - f_i^{eq}(\mathbf{x}, t)) + \Omega'_f, \quad (5)$$

$$g_i(\mathbf{x} + \mathbf{c}_i \Delta t, t + \Delta t) - g_i(\mathbf{x}, t) = -\frac{1}{\tau_g} (g_i(\mathbf{x}, t) - g_i^{eq}(\mathbf{x}, t)), \quad (6)$$

with the collision term (Ω'_f) being

$$\Omega'_f = \left(1 - \frac{1}{2\tau_f}\right) \frac{3\Delta t \omega_i}{c^2} \times (\mathbf{c}_i - \mathbf{u}) \cdot \left[\nabla \left(\frac{\rho c^2}{3} \right) \Gamma_i + (-\phi \nabla \cdot \lambda \mathbf{I} + \mathbf{F})(1 + \Gamma_i) \right], \quad (7)$$

$$\Gamma_i = \frac{3\mathbf{c}_i \cdot \mathbf{u}}{c^2} + \frac{9(\mathbf{c}_i \cdot \mathbf{u})^2}{2c^4} - \frac{3\mathbf{u} \cdot \mathbf{u}}{c^2}, \quad (8)$$

where subscript i is the discrete direction of the lattice velocity \mathbf{c}_i , \mathbf{x} is lattice position, Δt is the time step, ω_i is the related weight coefficient; f_i and g_i are the distribution functions, with f_i^{eq} and g_i^{eq} being the corresponding equilibrium distribution functions; τ_f and τ_g are the relaxation parameters.

According to the constitutive equation (4), the apparent kinematic viscosity ν is derived as

$$\tau \geq \tau_y : \quad \nu = \frac{\tau_y}{\rho \dot{\gamma}} + \frac{K}{\rho} \dot{\gamma}^{n-1}, \quad (9)$$

and it is closely related to the relaxation parameter τ_f in Eq. (5) as

$$\tau_f = \frac{1}{2} + \frac{3\nu}{c\Delta x}. \quad (10)$$

In addition, the shear rate $\dot{\gamma}$ is calculated by

$$\dot{\gamma} = (2|S_{\alpha\beta} S_{\beta\alpha}|)^{\frac{1}{2}}, \quad (11)$$

with the shear rate tensor $S_{\alpha\beta}$ calculated as

$$S_{\alpha\beta} = \frac{3}{2\rho\tau_f c^2} \sum_i f_i^{(1)} c_{i\alpha} c_{i\beta} \quad (12)$$

where the subscripts α, β are the spatial coordinates, $f_i^{(1)}$ is first order component of f_i in the Chapman-Enskog expansion. Thereafter, combining Eqs (9)–(12), the governing equation (4) is also encountered.

The validities of this model for capturing interface tension, static and dynamic contact angle, two-phase momentum evolution and two-phase relative permeability curve were well examined in previous works (Shao et al., 2014; Xie et al., 2016a, 2016b). It should be mentioned that in this approach, only local distribution functions are required, thus it avoids the complex differential processes in other direct simulation methods and improves accuracy to describe non-Newtonian behaviors.

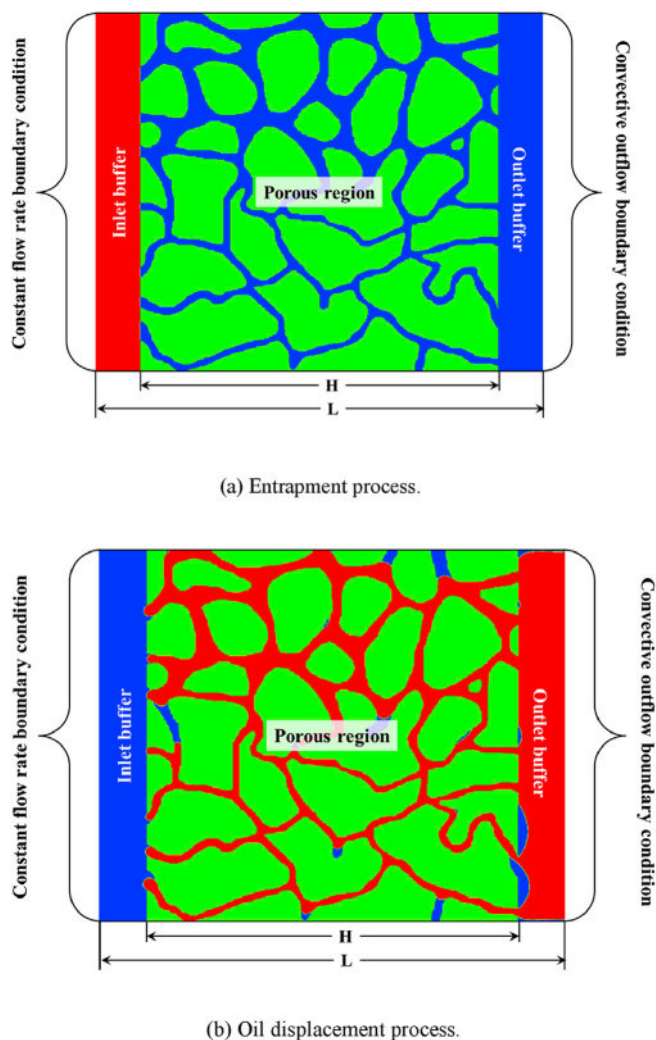


Fig. 1. Set-up of the computational domain and boundary conditions. Green represents the solid rock, red represents the oil and blue represents the displacing fluid. (For interpretation of the references to colour in this figure legend, the reader is referred to the web version of this article.)

2.3. Domain set-up and boundary conditions

The set-up of simulation domain in this work is described in Fig. 1, with red representing the oil, blue representing the displacing fluid and green representing the solid rock. The porous region occupies $H \times H$ lattices in the center of the whole domain with $L \times H$ lattices. We set two buffer regions beside the rock to minimize the possible inlet and outlet effects. In order to get an appropriate initial saturation distribution condition for the oil displacement process, we perform an entrapment process simulation beforehand, in which water is displaced by oil. At the beginning of the entrapment simulation, oil fills the inlet buffer region and water fills the rest as shown in Fig. 1a. Finally, a steady state will reach when the saturation distribution no longer changes, and this is set as the initial state for the displacing process with inlet buffer region replaced by displacing fluid as illustrated in Fig. 1b.

The upper and lower boundaries of the domain are set as solid walls to confine the flow, using the bounce-back rules as same as for the solid porous media. For the inlet, we set a constant flow rate condition applying the non-equilibrium extrapolation method (Guo and Chu-Guang, 2002). While for the outlet, we adopt the convective outflow boundary condition (Lou et al., 2013) which affects the main flow very slightly and is quite smooth for two-phase LBM outflow.

3. Comparisons between shear-thinning fluid and shear-thickening fluid for EOR

The performances of shear-thinning fluid and shear-thickening fluid as displacing fluid are comprehensively compared with each other in this section, together with water as a reference. As shown in Fig. 2 and Fig. 3, both homogeneous and heterogeneous 2D rock samples are considered, whose data is from experiments in Research Institute of Petroleum Exploration & Development (RIPEd). The sizes of these two samples are $0.15\text{mm} \times 0.15\text{mm}$ and $0.28\text{mm} \times 0.28\text{mm}$ respectively. By using the ordinary single LBM scheme, we get the sample permeability values as 543md and 428md with porosities being 34.15% and 25.45%. The heterogeneous sample is consist of two parts, one is the upper half with larger porosity of 32.01% and higher permeability of 691md , and the other is the lower half with smaller porosity of 18.89% and lower permeability of 147md .

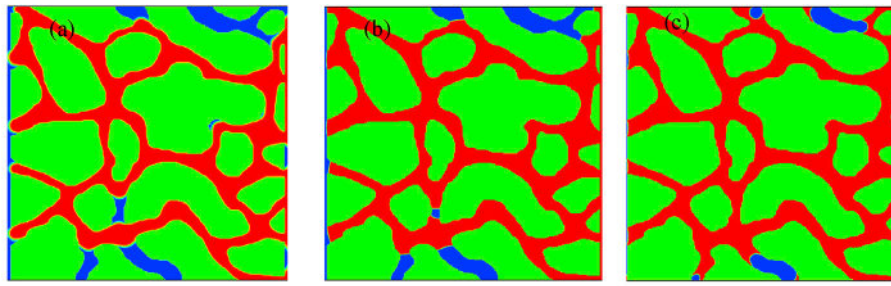
In our two-phase calculations, we use 300×300 lattices to cover the homogeneous sample with $L = 400$ for the whole domain; while for the heterogeneous cases, $H = 560$ and $L = 700$ are adopted. These sets ensure a relatively enough lattice number to capture the flow even in the narrowest channel. For other parameters, water density is $\rho_w = 1000\text{kg/m}^3$, kinematic viscosity is $\nu_w = 1 \times 10^{-6}\text{m}^2/\text{s}$; oil density is $\rho_o = 800\text{kg/m}^3$, kinematic viscosity is $\nu_o = 2.5 \times 10^{-5}\text{m}^2/\text{s}$; area flow rate is $Q = 6 \times 10^{-6}\text{m}^2/\text{s}$; interface tension is $\sigma = 0.01\text{N/m}$; and three kinds of wetting conditions including displacing fluid wet ($\theta = 60^\circ$), neutral wet ($\theta = 90^\circ$) and oil wet ($\theta = 120^\circ$) are considered.

Fig. 2 and Fig. 3 present phase distribution states for different wettabilities at their irreducible water saturations obtained by the entrapment simulations. As seen for both homogeneous and heterogeneous cases, the storage of oil increases with oil wettability, while the irreducible water saturation decreases. These phase distributions are then set as the initial states for the following displacement simulations.

3.1. Displacement through a homogeneous sample

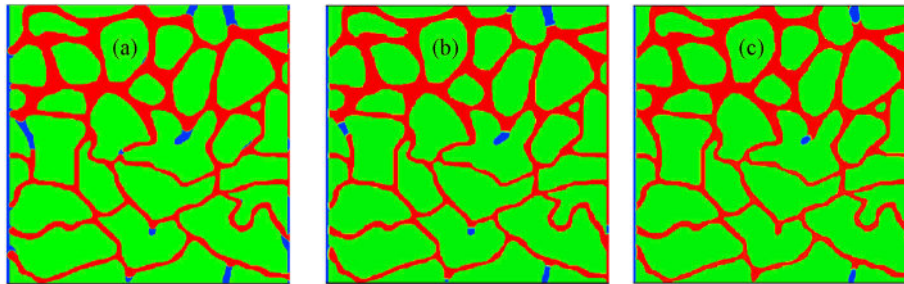
For oil displacement processes, we start with the homogeneous sample. In order to present strict comparisons, we divide it into two groups according to the viscosity ratio, one falls into favorable displacement regime, and the other is in unfavorable displacement regime. The oil viscosity is adopted as a reference viscosity to determine the parameters of non-Newtonian displacing fluids. In the first group, the effective apparent dynamic viscosities of both shear-thinning and shear-thickening fluids are kept higher than the reference viscosity during displacement. Flow indexes are set as $n = 0.7$ and 1.1 respectively for thinning and thickening fluids, consistency indexes and yield shear stresses are all set as $K = 1\text{Pa}\cdot\text{s}^n$ and $\tau_y = 1\text{Pa}$. While in the second group, the viscosities are lower with $K = 0.005\text{Pa}\cdot\text{s}^n$, $\tau_y = 0.01\text{Pa}$, $n = 0.8$ and 1.1 respectively. The effective apparent dynamic viscosities of non-Newtonian fluids are computed in a similar way with (Lopez et al., 2003), which are compared with the process of a Newtonian fluid flow through the same porous media.

We compare the evolution of oil and displacing fluid saturations for different wetting cases in Figs. 4–6. Pore volume (PV) of the displacing fluid is used to normalize the displacing time, which is defined as the cumulative injected fluid volume divided by the total space volume in rock sample. Both favorable and unfavorable displacements of non-Newtonian fluids are presented, with water flooding results as references. As is seen for all wetting cases, the saturation profiles of shear-thinning and shear-thickening fluid displacements are almost coincide with each other in favorable displacement regime, showing better recovery performance over water flooding. However, in unfavorable displacement regime, they deviate from each other, and the shear-thinning profiles approach water flooding results, showing poorer performance. This can be attributed to the crucial impact of viscosity ratio on fluid instability in unfavorable displacements, for any variance could



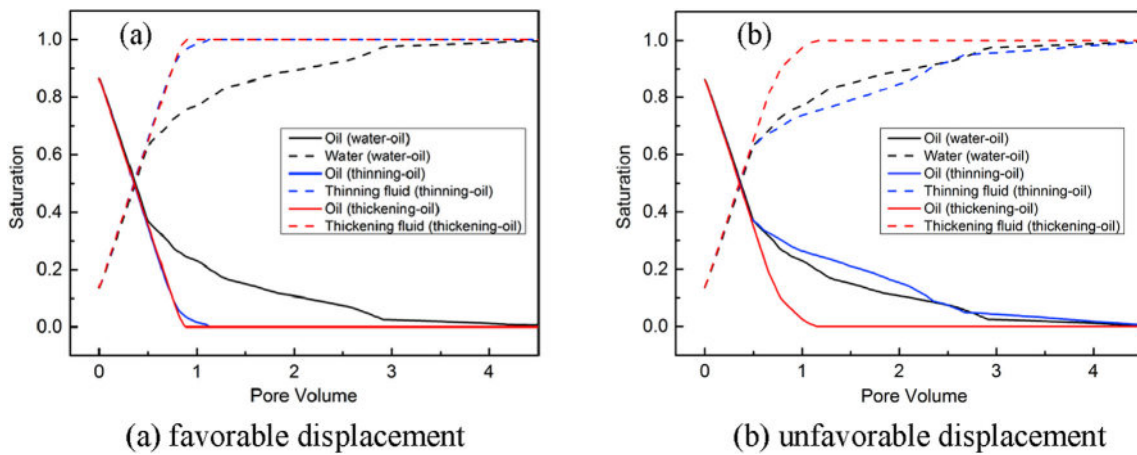
(a) displacing fluid wet ($\theta = 60^\circ$) (b) neutral wet ($\theta = 90^\circ$) (c) oil wet ($\theta = 120^\circ$)

Fig. 2. Initial states for displacement processes obtained at the end of entrapment simulations for the homogeneous rock sample.



(a) displacing fluid wet ($\theta = 60^\circ$) (b) neutral wet ($\theta = 90^\circ$) (c) oil wet ($\theta = 120^\circ$)

Fig. 3. Initial states for displacement processes obtained at the end of entrapment simulations for the heterogeneous rock sample.



(a) favorable displacement

(b) unfavorable displacement

Fig. 4. Comparisons of saturation evolutions in homogeneous rock under displacing fluid wet ($\theta = 60^\circ$) condition.

make a negligible difference in recovery; while for favorable displacements in homogeneous rock, it is not that important since the displacements are already stable once the ratio decreases to 1. In Fig. 7, we take the phase distributions at 0.7 PV during displacements under displacing fluid wet ($\theta = 60^\circ$) condition as an illustration. Almost uniform displacing fronts are found for two favorable displacements; while there begins to appear somewhat instable for shear-thickening displacement in unfavorable regime, and it is more severe for shear-thinning displacement. The extent of instability is closely related to the dynamic viscosity ratio between oil and displacing fluid, as we obtain the ratios for water flooding, shear-thinning and shear-thickening displacement in unfavorable regime to be 20, 43.9, and 1.27 respectively.

Therefore, the EOR performance of shear-thinning and shear-thickening fluid in homogeneous reservoir should be concluded as follows. When the apparent viscosities of both fluids are much higher than

oil, it will lead to stable displacements which are not sensitive to viscosity ratio, and the final oil recovery will be almost the same. However, when they are in unfavorable displacement regime, the front instability is sensitive to viscosity ratio, thus shear-thickening fluid is preferred to achieve smaller viscosity ratio and stable recovery.

3.2. Displacement through a heterogeneous sample

Further, oil displacements in the heterogeneous sample are investigated, with special emphasis on the diversion effect. In this subsection, we refine our discussions in the favorable displacement regime, since the instability of shear-thinning fluid can be even worse for heterogeneous reservoir. Thus parameters of $K = 1Pa \cdot s^n$, $\tau_y = 1Pa$, $n = 0.7$ and 1.1 respectively for thinning and thickening fluids are applied.

Displacement processes under displacing fluid wet ($\theta = 60^\circ$) condi-

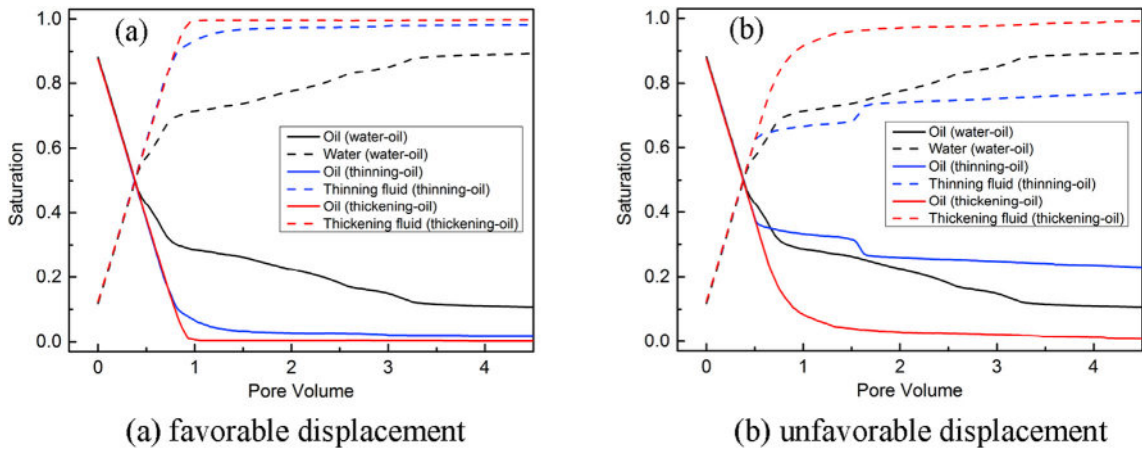


Fig. 5. Comparisons of saturation evolutions in homogeneous rock under neutral wet ($\theta = 90^\circ$) condition.

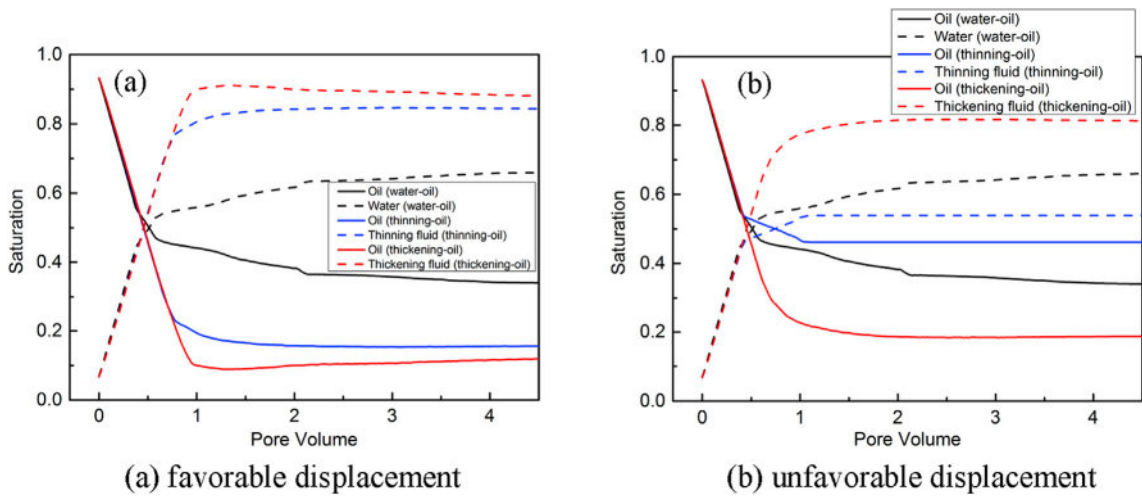


Fig. 6. Comparisons of saturation evolutions in homogeneous rock under oil wet ($\theta = 120^\circ$) condition.

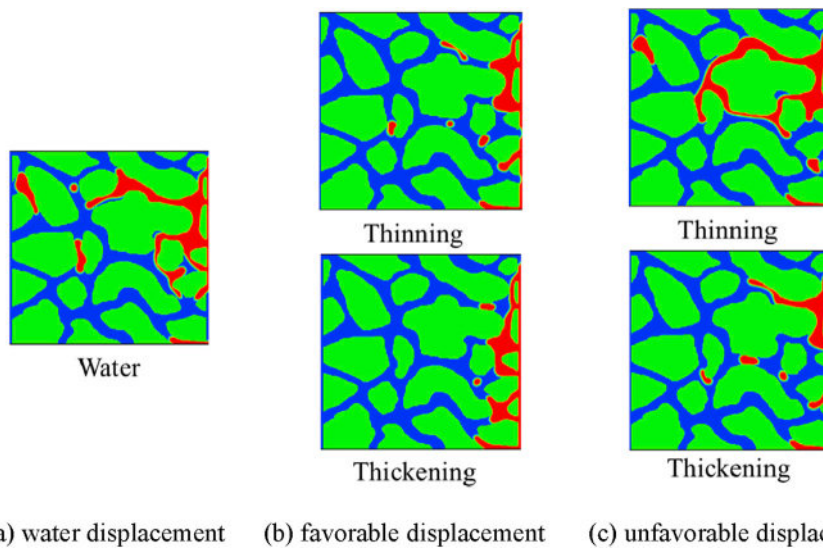


Fig. 7. Comparisons of phase distributions at 0.7 PV during displacements under displacing fluid wet ($\theta = 60^\circ$) condition for the homogeneous rock sample. (a) Water flooding result as a reference; (b) non-Newtonian fluid displacement in favorable regime; (c) non-Newtonian fluid displacement in unfavorable regime.

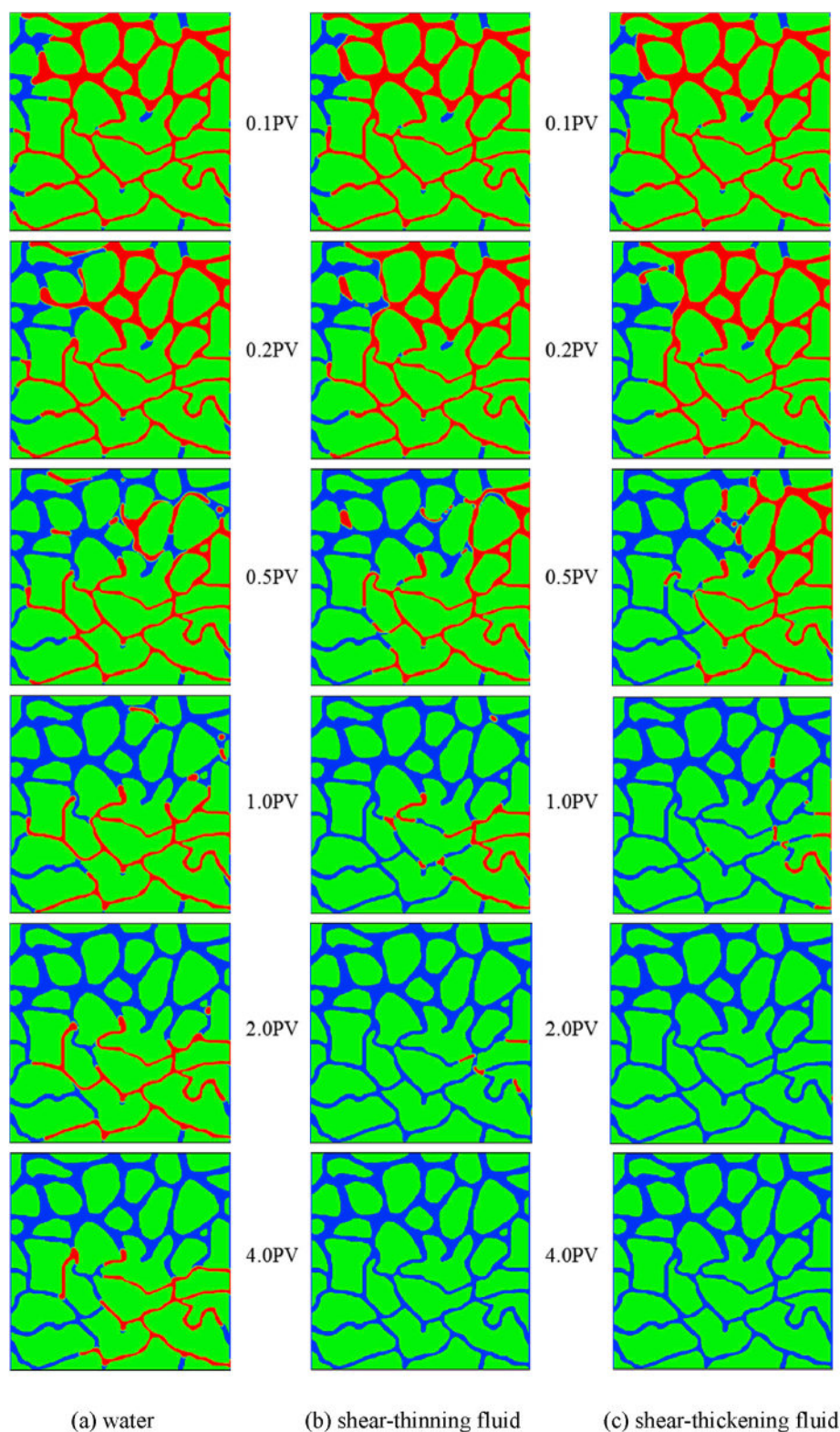


Fig. 8. Comparisons of phase distributions during displacement under displacing fluid wet ($\theta = 60^\circ$) condition for the heterogeneous rock sample. (a) Water flooding result as a reference; (b) shear-thinning fluid displacement in favorable regime; (c) shear-thickening fluid displacement in favorable regime.

tion are presented in Fig. 8 as an illustration. From the water flooding process, the preferential behavior of water is notably observed, in which most water tends to travel through the high permeable layer and forms some main flow paths confined in that region. As a result, the oil deposited in the low permeable layer is hard to recover, even though the injected volume of water reaches 4 PV. Compared with water, both the

shear-thinning fluid and the shear-thickening fluid exhibit diversion effect, which makes the displacing front more stable and improves the oil recovery in low permeable layer. Moreover, the diversion capability of shear-thickening fluid is found to be stronger than the shear-thinning fluid, according to the comparisons time by time. These are also coincident with our quantitative results of oil saturation and sweep efficiency

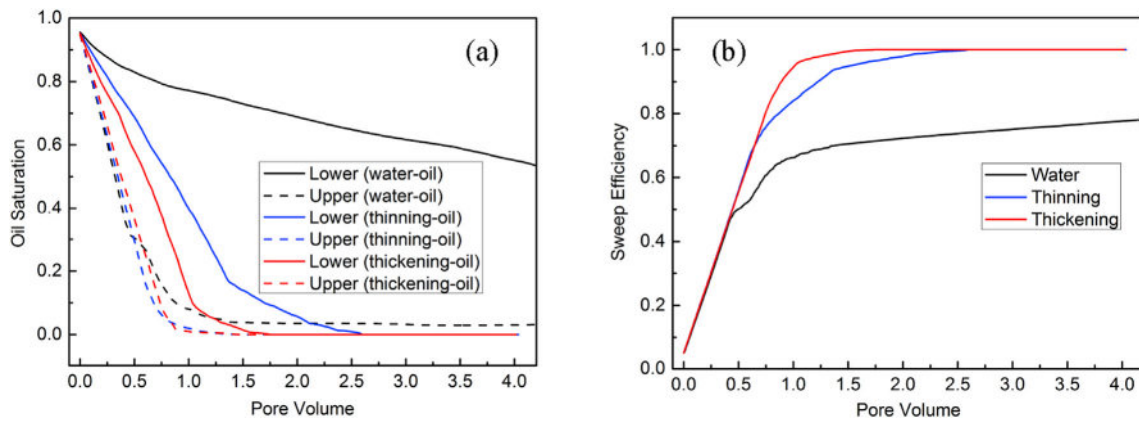


Fig. 9. The evolutions of (a) oil saturation in upper and lower part of the heterogeneous rock; and (b) total sweep efficiency under displacing fluid wet ($\theta = 60^\circ$) condition.

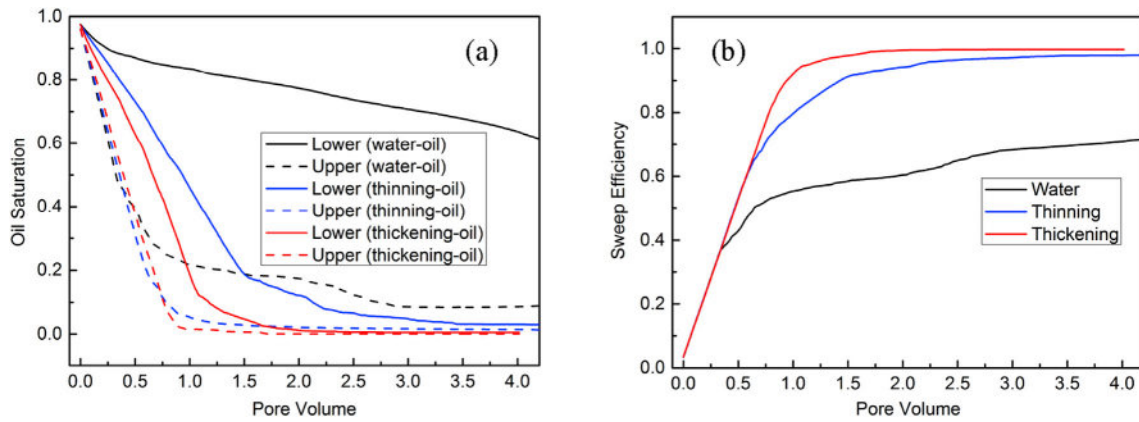


Fig. 10. The evolutions of (a) oil saturation in upper and lower part of the heterogeneous rock; and (b) total sweep efficiency under neutral wet ($\theta = 90^\circ$) condition.

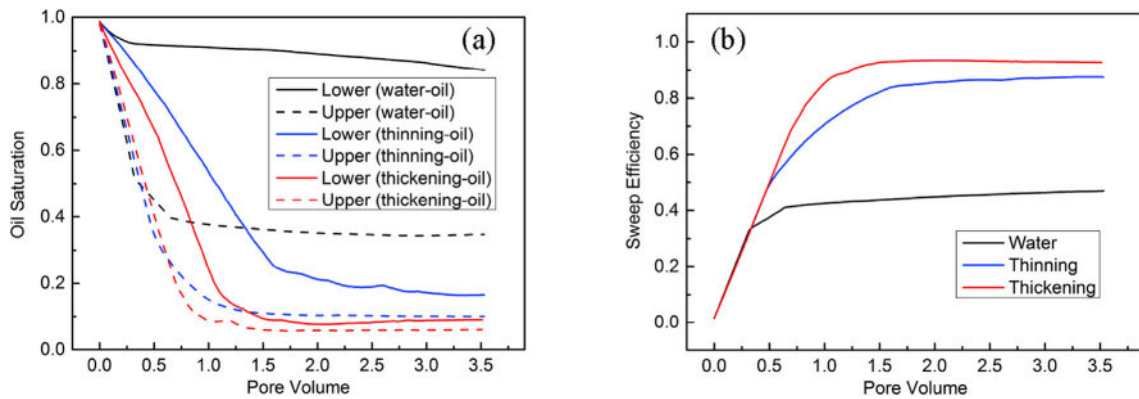


Fig. 11. The evolutions of (a) oil saturation in upper and lower part of the heterogeneous rock; and (b) total sweep efficiency under oil wet ($\theta = 120^\circ$) condition.

for different wetting conditions. In Figs. 9a, 10a and 11a, evolutions of oil saturation are compared, the discrepancy between the upper (dash lines) and lower oil saturation (solid lines) represents the diversion extent, and smaller discrepancy means stronger diversion. In Figs. 9b, 10b and 11b, the total sweep efficiency evolutions are compared, which represent the oil recovery capability. All of these figures indicate the EOR performance of shear-thickening fluid is the best in heterogeneous reservoir, and it is most strikingly observed in oil wet case, which is usually the toughest condition for oil recovery. The main reason for this still lies in the dynamic viscosity ratios, which are 0.078, 0.865 and 20 respectively for shear-thickening, shear-thinning and water displacing cases, as the smallest value is found for shear-thickening displacement.

Therefore, for heterogeneous reservoir, even though both of the fluids are in favorable displacement regime, the shear-thickening fluid is better for EOR due to its higher viscosity and corresponding stronger diversion evidence. These results also indicate that the shear-thinning behavior does not contribute too much on diversion, and it is still the viscosity ratio really matters. It is noted that this conclusion may conflict somewhat with the suppositions in Ref (Zhang et al., 2000), discussing about foam diversion. This is because they assumed almost the same velocities in small and large throats, then by using the definition of shear rate, a smaller throat will lead to a larger shear rate and a relative smaller resistance for shear-thinning fluid. However, it is not usually the case under ordinary conditions, the velocities in smaller throat are also

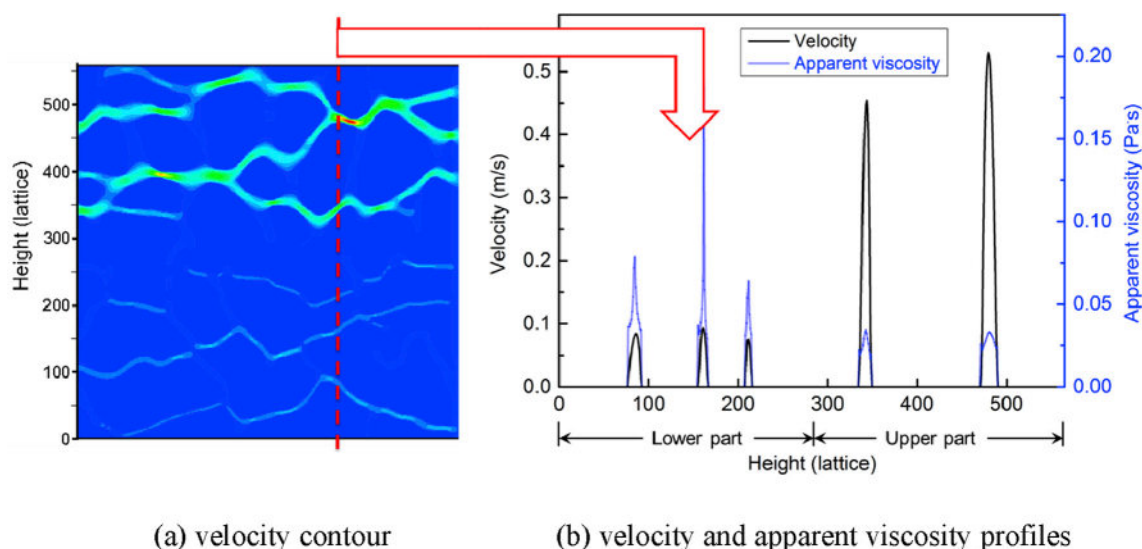


Fig. 12. Extraction of the cross-sectional velocity and apparent viscosity profiles from shear-thinning fluid displacement process at 4 PV under displacing fluid wet ($\theta = 60^\circ$) condition.

smaller, resulting in smaller shear rate and larger viscosities. See Fig. 12, for instance, where we extract the pore-scale info of cross-sectional velocities and apparent viscosities from shear-thinning fluid displacement process. It is clear that the velocities of shear-thinning fluid in the upper part are larger than that in the lower part, while the apparent viscosity distribution is opposite. As a consequence, despite the shear-thinning behavior of foam, its diversion effect should be majorly ascribed to other reasons like the surfactant concentration (Al Ayesh et al., 2016): most surfactants are tend to get into the higher permeable layer and form more foams there, thus will increase the viscosity and divert flows to lower permeable layer.

It is worth mentioning that although smaller viscosity ratio can provide more stable displacement and improve the sweep efficiency, it will also bring much more energy cost due to the increase of viscous resistance. As a consequence, to achieve a better recovery with economic considerations, it is necessary to find a balanced choice between sweep efficiency and energy cost.

4. Conclusions

Direct pore-scale modeling of non-Newtonian fluid displacement in porous media is performed by using a multiphase LBM model for viscoplastic fluid flow. The roles of shear-thinning and shear-thickening properties in oil recovery are studied by displacement simulations in both homogeneous and heterogeneous rock samples.

For homogeneous cases, in order to make strict comparisons, we divide two regimes based on the viscosity ratio, one is the favorable displacement regime, and the other is the unfavorable regime. In the favorable regime where the mean apparent dynamic viscosities of non-Newtonian displacing fluids are higher than the oil viscosity, the oil productions are almost the same for shear-thinning and shear-thickening displacements. While in the unfavorable regime, shear-thickening fluid should be applied for its better stability. For heterogeneous cases, the performance of shear-thinning fluid is found to be poorer than shear-thickening fluid although compared in the favorable displacement regime. We further extract the cross-sectional velocity and apparent viscosity profiles during shear-thinning fluid displacement process, and found that the relative magnitudes of velocities and viscosities in throats with different sizes do not follow the same descriptions as in some previous suppositions. These results demonstrate merely shear-thinning property does not enhance the diversion effect as supposed. Its essence should still lie mainly in the viscosity ratio and in other properties of foam or specific polymer as well. However, smaller viscosity ratio will

cause much more energy cost, therefore further efforts are expected to promote a balanced choice between final oil production and energy cost.

Acknowledgments

This work is financially supported by the NSF grant of China (No. 51676107, U1562217), National Science and Technology Major Project on Oil and Gas (No.2017ZX05013001), PetroChina Innovation Foundation (No. 2015D-5006-0201) and the Tsinghua University Initiative Scientific Research Program (No. 2014z22074).

References

- Abdulbaki, M., Huh, C., Sepehrnoori, K., Delshad, M., Varavei, A., 2014. A critical review on use of polymer microgels for conformance control purposes. *J. Petroleum Sci. Eng.* 122, 741–753.
- Al Ayesh, A.H., Salazar, R., Farajzadeh, R., Vincent-Bonnieu, S., Rossen, W.R., 2016. Foam diversion in heterogeneous reservoirs: effect of permeability and injection method. In: *SPE Improved Oil Recovery Conference. SPE-199650-MS*, Tulsa, Oklahoma, USA.
- AlSofi, A.M., Blunt, M.J., 2010. Streamline-based simulation of non-Newtonian polymer flooding. *SPE 15 (04)*, 895–905.
- Alvarado, V., Manrique, E., 2010. Enhanced oil recovery: an update review. *Energies* 3 (9), 1529–1575.
- Andrianov, A., Farajzadeh, R., Mahmoodi Nick, M., Talanana, M., Zitha, P.L.J., 2012. Immiscible foam for enhancing oil recovery: bulk and porous media experiments. *Industrial Eng. Chem. Res.* 51 (5), 2214–2226.
- Bai, Y., et al., 2015. Gelation study on a hydrophobically associating polymer/polyethylenimine gel system for water shut-off treatment. *Energy Fuels* 29 (2), 447–458.
- Cahn, J.W., Hilliard, J.E., 1958. Free energy of a nonuniform system. I. interfacial free energy. *J. Chem. Phys.* 28 (2), 258–267.
- Delshad, M., et al., 2008. Mechanistic Interpretation and Utilization of Viscoelastic Behavior of Polymer Solutions for Improved Polymer-flood Efficiency. *SPE 113620*.
- Farajzadeh, R., Andrianov, A., Zitha, P.L.J., 2010. Investigation of immiscible and miscible foam for enhancing oil recovery. *Industrial Eng. Chem. Res.* 49 (4), 1910–1919.
- Guo, Z.-L., Chu-Guang, Z., 2002. Non-equilibrium extrapolation method for velocity and pressure boundary conditions in the lattice Boltzmann method. *Chin. Phys.* 11 (4), 366.
- He, J.Y., et al., 2008. Size effect on mechanical properties of micron-sized PS-DVB polymer particles. *Polymer* 49 (18), 3993–3999.
- Herschel, W.H., Bulkley, R., 1926. Konsistenzmessungen von Gummi-Benzollösungen. *Kolloid-Zeitschrift* 39 (4), 291–300.
- Huang, H., Sukop, M., Lu, X., 2015. *Multiphase Lattice Boltzmann Methods: Theory and Application*. John Wiley & Sons.
- Huang, J.J., Shu, C., Chew, Y.T., 2009. Mobility-dependent bifurcations in capillarity-driven two-phase fluid systems by using a lattice Boltzmann phase-field model. *Int. J. Numer. Methods Fluids* 60 (2), 203–225.
- Jones, W.M., 1980. Polymer additives in reservoir flooding for oil recovery: shear thinning or shear thickening? *J. Phys. D Appl. Phys.* 13 (5), L87.
- Jung, J.C., Zhang, K., Chon, B.H., Choi, H.J., 2013. Rheology and polymer flooding characteristics of partially hydrolyzed polyacrylamide for enhanced heavy oil recovery. *J. Appl. Polym. Sci.* 127 (6), 4833–4839.

- Li, R.F., Yan, W., Liu, S., Hirasaki, G., Miller, C.A., 2010. Foam mobility control for surfactant enhanced oil recovery. *SPE* 15 (04), 928–942.
- Liu, H., et al., 2015a. Multiphase lattice Boltzmann simulations for porous media applications. *Comput. Geosci.* 1–29.
- Liu, Y., Zhong, H., Peng, X., Zhao, C., 2015b. Factors influencing micro sweep efficiency when flooding a formation with viscoelastic polymer solutions. *Chem. Technol. Fuels Oils* 51 (2), 160–167.
- Lopez, X., Valvatne, P.H., Blunt, M.J., 2003. Predictive network modeling of single-phase non-Newtonian flow in porous media. *J. Colloid Interface Sci.* 264 (1), 256–265.
- Lou, Q., Guo, Z., Shi, B., 2013. Evaluation of outflow boundary conditions for two-phase lattice Boltzmann equation. *Phys. Rev. E* 87 (6), 063301.
- Morais, A.F., Seybold, H., Herrmann, H.J., Andrade, J., 2009. Non-newtonian fluid flow through three-dimensional disordered porous media. *Phys. Rev. Lett.* 103 (19), 194502.
- Ohta, M., Nakamura, T., Yoshida, Y., Matsukuma, Y., 2011. Lattice Boltzmann simulations of viscoplastic fluid flows through complex flow channels. *J. Newt. Fluid Mech.* 166 (7–8), 404–412.
- Raeini, A.Q., Blunt, M.J., Bijeljic, B., 2014. Direct simulations of two-phase flow on micro-CT images of porous media and upscaling of pore-scale forces. *Adv. Water Resources* (74), 116–126.
- Shao, J.Y., Shu, C., Huang, H.B., Chew, Y.T., 2014. Free-energy-based lattice Boltzmann model for the simulation of multiphase flows with density contrast. *Phys. Rev. E* 89 (3), 033309.
- Talebian, S.H., Masoudi, R., Tan, I.M., Zitha, P.L.J., 2014. Foam assisted CO₂-EOR: a review of concept, challenges, and future prospects. *J. Petroleum Sci. Eng.* 120, 202–215.
- Thomas, S., 2008. Enhanced oil recovery - an overview. *Oil Gas Sci. Technol. - Rev. IFP* 63 (1), 9–19.
- Wang, D., et al., 2000. Viscous-elastic Polymer Can Increase Microscale Displacement Efficiency in Cores. SPE-63227-MS.
- Wei, B., Romero-Zer, Rodrigue, D., 2014. Oil displacement mechanisms of viscoelastic polymers in enhanced oil recovery (EOR): a review. *J. Petroleum Explor. Prod. Technol.* 4 (2), 113–121.
- Wever, D.A.Z., Picchioni, F., Broekhuis, A.A., 2011. Polymers for enhanced oil recovery: a paradigm for structure-property relationship in aqueous solution. *Prog. Polym. Sci. Top. Energy Relat. Mater.* 36 (11), 1558–1628.
- Xie, C., Zhang, J., Bertola, V., Wang, M., 2016a. Droplet evaporation on a horizontal substrate under gravity field by mesoscopic modeling. *J. Colloid Interface Sci.* 463, 317–323.
- Xie, C., Zhang, J., Bertola, V., Wang, M., 2016b. Lattice Boltzmann modeling for multiphase viscoplastic fluid flow. *J. Newt. Fluid Mech.* 234, 118–128.
- Yan, W., Miller, C.A., Hirasaki, G.J., 2006. Foam sweep in fractures for enhanced oil recovery. *Colloids Surfaces A Physicochem. Eng. Aspects* 282–283, 348–359.
- Zhang, Y., Yue, X., Dong, J., Yu, L., 2000. New and Effective Foam Flooding to Recover Oil in Heterogeneous Reservoir. SPE-59367-MS.
- Zhang, Z., Li, J., Zhou, J., 2011. Microscopic roles of “viscoelasticity” in HPMA polymer flooding for EOR. *Transp. Porous Media* 86 (1), 199–214.
- Zhu, J.J., Ma, J.S., 2013. An improved gray lattice Boltzmann model for simulating fluid flow in multi-scale porous media. *Adv. Water Resour.* 56, 61–76.
- Zhu, T., Strycker, A., Raible, C.J., Vineyard, K., 1998. Foams for Mobility Control and Improved Sweep Efficiency in Gas Flooding. SPE 39680.